

pubs.acs.org/NanoLett Letter

Highly Selective Electrochemical Nitrate to Ammonia Conversion by Dispersed Ru in a Multielement Alloy Catalyst

Meiqi Yang,[†] Boyang Li,[†] Shuke Li,[†] Qi Dong, Zhennan Huang, Sunxiang Zheng, Ying Fang, Guangye Zhou, Xi Chen, Xiaobo Zhu, Tangyuan Li, Miaofang Chi, Guofeng Wang,* Liangbing Hu,* and Zhiyong Jason Ren*



Cite This: Nano Lett. 2023, 23, 7733-7742



ACCESS

Metrics & More

Article Recommendations

s Supporting Information

ABSTRACT: Electrochemical reduction of nitrate to ammonia (NH₃) converts an environmental pollutant to a critical nutrient. However, current electrochemical nitrate reduction operations based on monometallic and bimetallic catalysts are limited in NH₃ selectivity and catalyst stability, especially in acidic environments. Meanwhile, catalysts with dispersed active sites generally exhibit a higher atomic utilization and distinct activity. Herein, we report a multielement alloy nanoparticle catalyst with dispersed Ru (Ru-MEA) with other synergistic components (Cu, Pd, Pt). Density functional theory elucidated the synergy effect of Ru-MEA than Ru, where a better reactivity (NH₃ partial current density of



 -50.8 mA cm^{-2}) and high NH₃ faradaic efficiency (93.5%) is achieved in industrially relevant acidic wastewater. In addition, the Ru-MEA catalyst showed good stability (e.g., 19.0% decay in FE_{NH3} in three hours). This work provides a potential systematic and efficient catalyst discovery process that integrates a data-guided catalyst design and novel catalyst synthesis for a range of applications.

KEYWORDS: electrochemical nitrate reduction, ammonia, multielement alloy catalyst, industrial wastewater, acidic

he global nitrogen (N) cycle has been largely altered by human activities in the past century, resulting in severe energy and environmental problems.^{1,2} In the N cycle, nitrate (NO₃⁻) is a major contaminant from industrial effluents and is typically converted to N2 gas through biological denitrification (Figure 1a).^{3,4} This process is not economically efficient and is associated with potent greenhouse gas nitrous oxide (N2O) emissions.⁵⁻⁸ However, many of these liquid wastes (e.g., fertilizer, ammunition, metal pickling, and nuclear industries) are acidic at their source of generation due to the consumption of nitric acid and have very low biodegradability; thus, chemical addition or pretreatment is necessary for NO₃ removal and discharge. 9-12 Ammonia (NH₃) is another critical component of the cycle and an essential fertilizer and chemical feedstock. 13 NH₃ is mostly synthesized using N₂ and H₂ by the energy-intensive Haber Bosch process, which accounts for 1.8% of global energy consumption and 1.4% of global CO₂ emissions.¹⁴ During utilization, the NH₃ is generally oxidized to NO₃⁻, and decades of overfertilization and releases of these nitrogen pollutants in the water body have been a major cause of eutrophication, biodiversity loss, and N₂O emissions. 15 Therefore, rather than finishing the N cycle via N2 using high cost of energy and chemicals, a shortcut reduction directly from NO₃⁻ to NH₃ holds the promise to reduce nitrogen pollution while producing green and distributed NH3 (Figure 1a).^{16–18}

To catalyze electrochemical NO₃⁻ reduction (ENR), a range of monometallic catalysts made by transition metals such as Ru, Rh, Pt, Pd, Ti, Cu, 19-21 and bimetallic catalysts such as Pd-Cu,²² Pt-Ir,²³ Pt-Pd,²⁴ Pt-Ru,²⁵ Cu-Ni²⁶ have been extensively studied. However, monometallic catalysts generally exhibit low ENR activity since the single metal site is incapable of accommodating multiple reaction intermediate steps. Compared to monometallic materials, bimetallic alloy catalysts often show enhanced performance (i.e., activity and selectivity), but these catalysts are still limited in their product selectivity and long-term stability since the lack of compositional tunability and limited synergy.^{27,28} Metal-free catalysts, such as graphite felt,²⁹ amorphous graphene,³⁰ and activecarbon fiber paper,31 are potential alternatives, particularly suitable for operating under extreme conditions (e.g., acidic environment) due to their strong corrosion resistance, wide operation potential range, and comparable selectivity. However, metal-free catalysts still face some major barriers in achieving competitive reaction efficiencies compared with

Received: May 29, 2023 **Revised:** June 19, 2023 **Published:** June 28, 2023





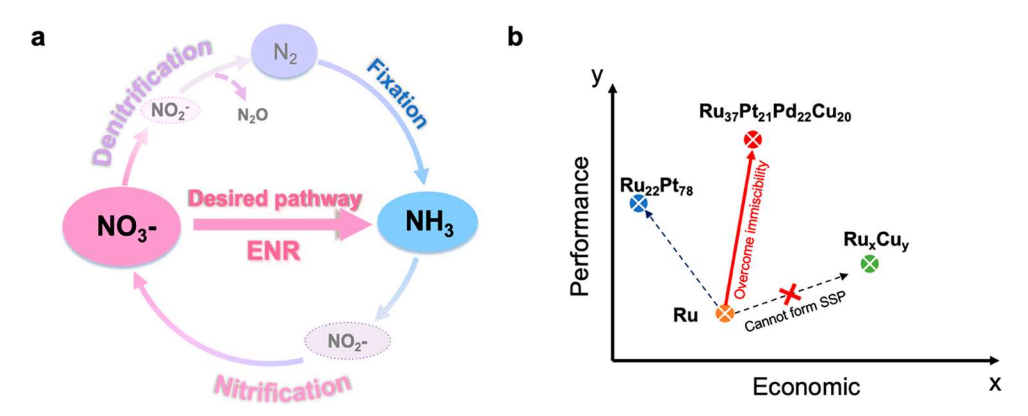


Figure 1. (a) Schematic diagram of the traditional nitrogen conversion cycle consisting of nitrification, denitrification, and N_2 fixation (greyed), and the reported direct electrocatalytic NO_3^- reduction (ENR) to NH_3 in this work. (b) Design principle of MEA NP ($Ru_{37}Pt_{21}Pd_{22}Cu_{20}$) catalyst based on a benchmark Ru catalyst, where SSP indicates a solid solution phase.

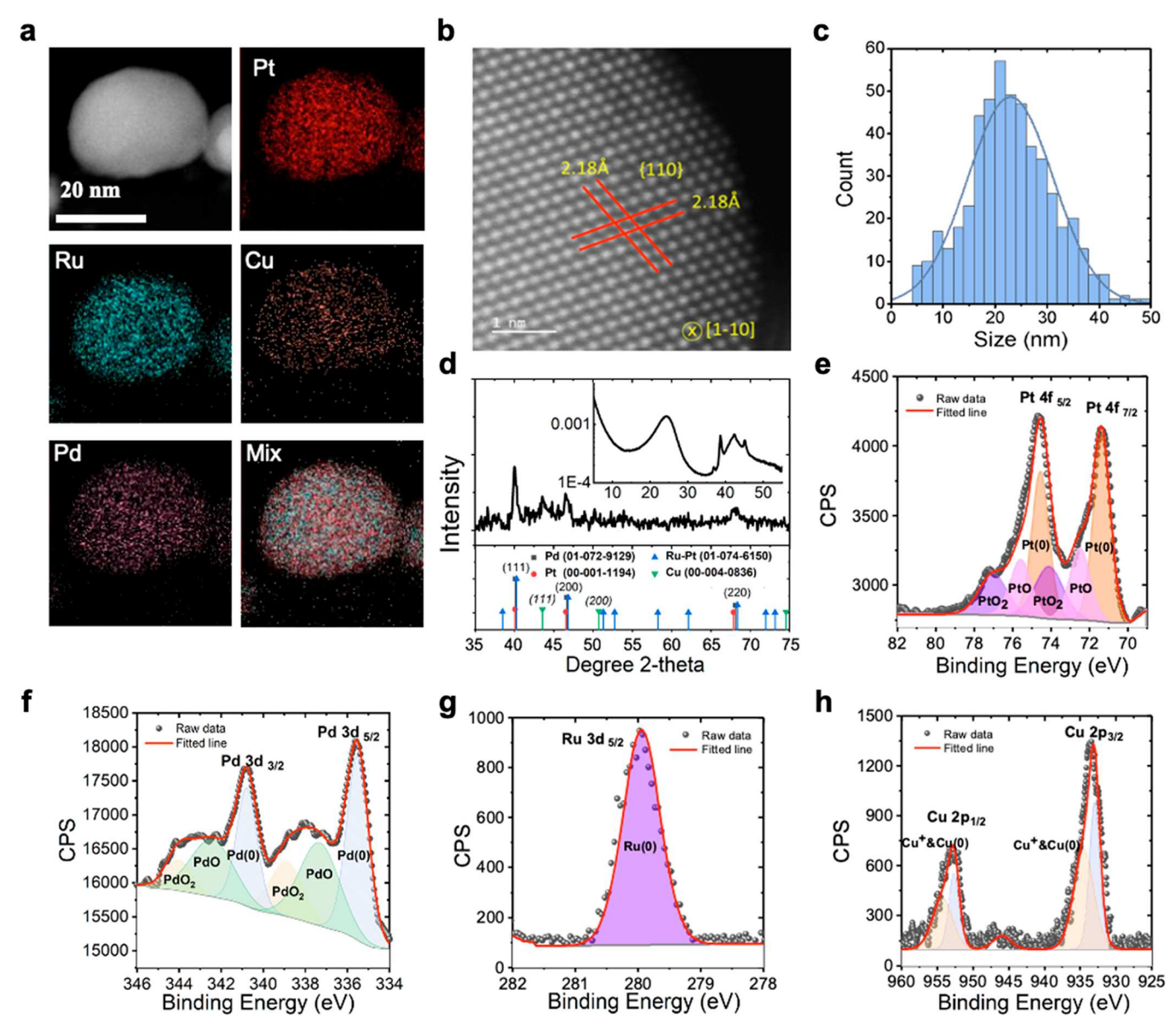


Figure 2. Characterization of the Ru-MEA NPs: (a) STEM elemental maps for Ru-MEA NPs. (b) HAADF image. (c) Catalysts' size distribution was generated from the SEM spectrum and the fitted normal distribution (details in Supporting Information). (d) XRD pattern and SAXS data of Ru-MEA with labeled phases corresponding to reference standards of Pd/Pt/RuPt and Cu (italic). XPS core level scan of each component in Ru-MEA NPs: (e) Pt 4f, (f) Pd 3d, (g) Ru 3d_{5/2}, (h) Cu 2p.

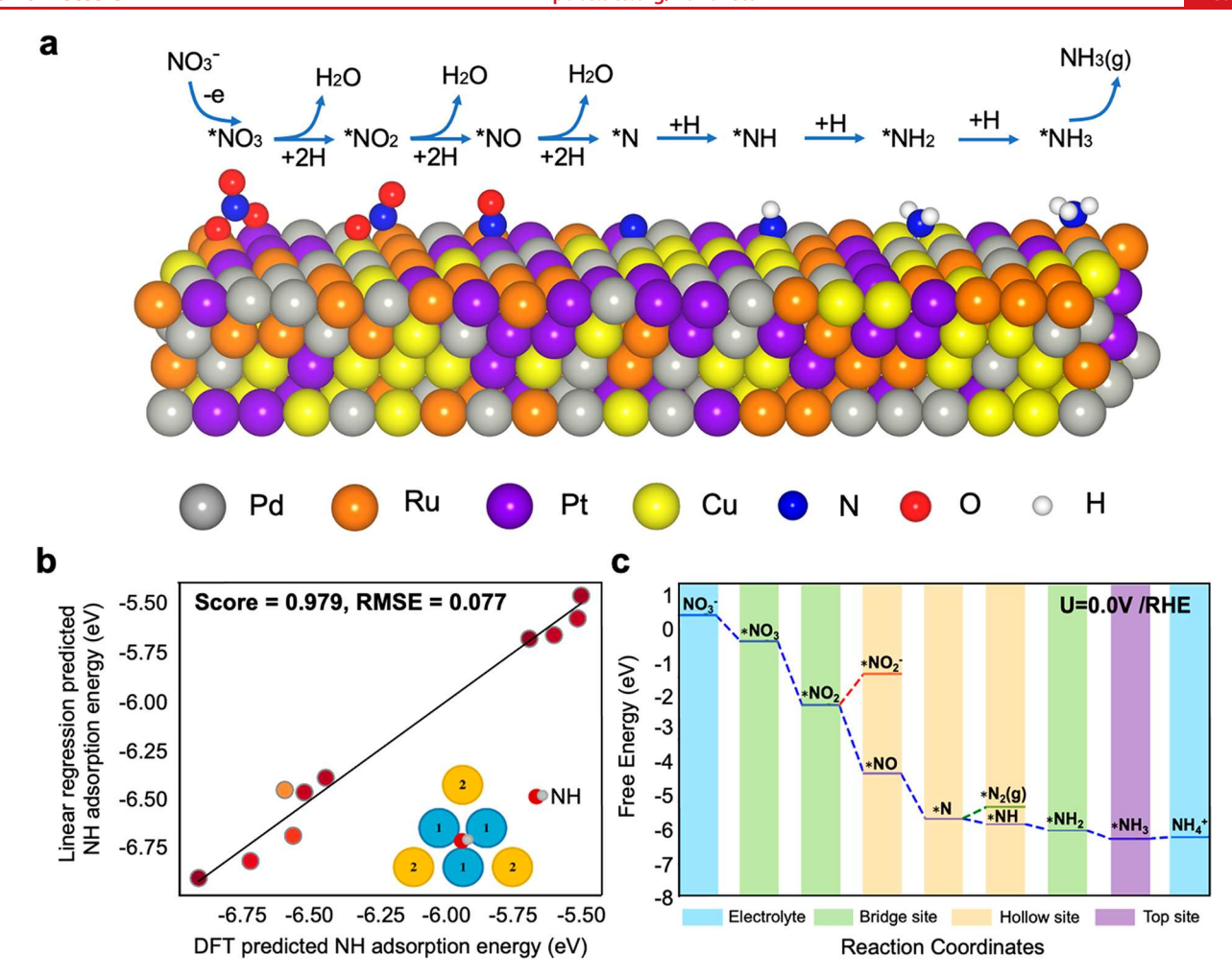


Figure 3. (a) Proposed NO_3^- reduction reaction pathway to NH_3 on the RuPtPdCu (111) surface. In the figure, the gray, orange, purple, yellow, blue, red, and white balls represent Pd, Ru, Pt, Cu, N, O, and H atoms, respectively. (b) DFT predicted the adsorption energy as compared to the adsorption energy predicted by the linear regression model, which links the local chemical environment of the surface sites and NH adsorption energy. The inset shows that an NH is adsorbed on a surface site on RuPtPdCu (111) containing the three nearest neighboring metal atoms (i.e., the blue balls marked with "1") and three second-neighboring metal atoms (i.e., the yellow balls marked with "2"). (c) Predicted free energy evolution for NO_3^- to NH_3 (blue line), NO_2^- (red line), and N_2 (green line). In this figure, the NO_3^- reduction intermediates highlighted by the blue shadow are dispersed in the electrolyte, and the NO_3^- reduction intermediates highlighted by the green, orange, and purple shadows are adsorbed on a bridge site, hollow site, and top site on RuPtPdCu (111), respectively.

metal catalysts. In the case of metallic catalysts, compared with bulk structures, dispersing transition metal atoms into isolated sites exhibit extraordinary advantages, such as higher atomic utilization, enhanced activity, and high selectivity. 32,33 However, this generally requires advanced fabrication methods, is difficult to extend to all metal species, and is immature for binary and ternary compositions.³⁴ More importantly, among the catalysts studied to date, few candidates have shown satisfying ENR activity nor high NH3 faradaic efficiency (FE_{NH3}) in acidic conditions $(FE_{NH3} = 78\%, i_{NH3} = 22 \text{ mA})$ cm⁻² on Ti foil),³⁵ which are industrially relevant. On the one hand, some high-strength NO₃⁻ waste streams from industry are in acidic environments (pH 2-3) at their source of generation. 10,11,36 On the other hand, conducting ENR in acidic conditions promises better practicality, where acidic electrolyte enables the use of proton-exchange membranes to permit higher current densities.³⁷ Therefore, developing highly efficient catalysts to enable ENR under acidic conditions becomes an imperative task.

In this study, we report the first multielement alloy (MEA) nanoparticles (NPs) with dispersed Ru atoms (Ru-MEA) for

highly selective and stable ENR to NH3 in industrially relevantacidic wastewater conditions. The Ru-MEA catalyst is developed upon the benchmark Ru catalyst, where an additional synergy effect is achieved by dispersing Ru with other metals to form alloy NPs. 38,39 Cu is selected to mix with Ru due to its activity for NO₃ reduction and to potentially reduce Ru usage. 21,40 However, Ru and Cu are conventionally immiscible even above the melting point according to their wide miscibility gaps in the phase diagrams. 41-43 Pt and Pd are added to realize the homogeneous alloying between Ru and Cu. Besides, synergies in bimetallic catalysts such as RuPt, PtCu, PtPd, and PdCu have been widely studied. 25,44-47 Therefore, the addition of Pt and Pd not only serves as the "glue" to overcome the immiscibility between Ru and Cu and form MEA but also further enhances the reaction activity (Figure 1b). Using thermal shock, we are able to synthesize Ru-MEA NPs in a solid solution state in a simple manner and achieve homogeneous Ru dispersion. 48 In Ru-MEA, the uniform mixing of Ru, Pd, Pt, and Cu has the potential to create numerous favorable surface binding sites. The interactions between adjacent elements could modify their

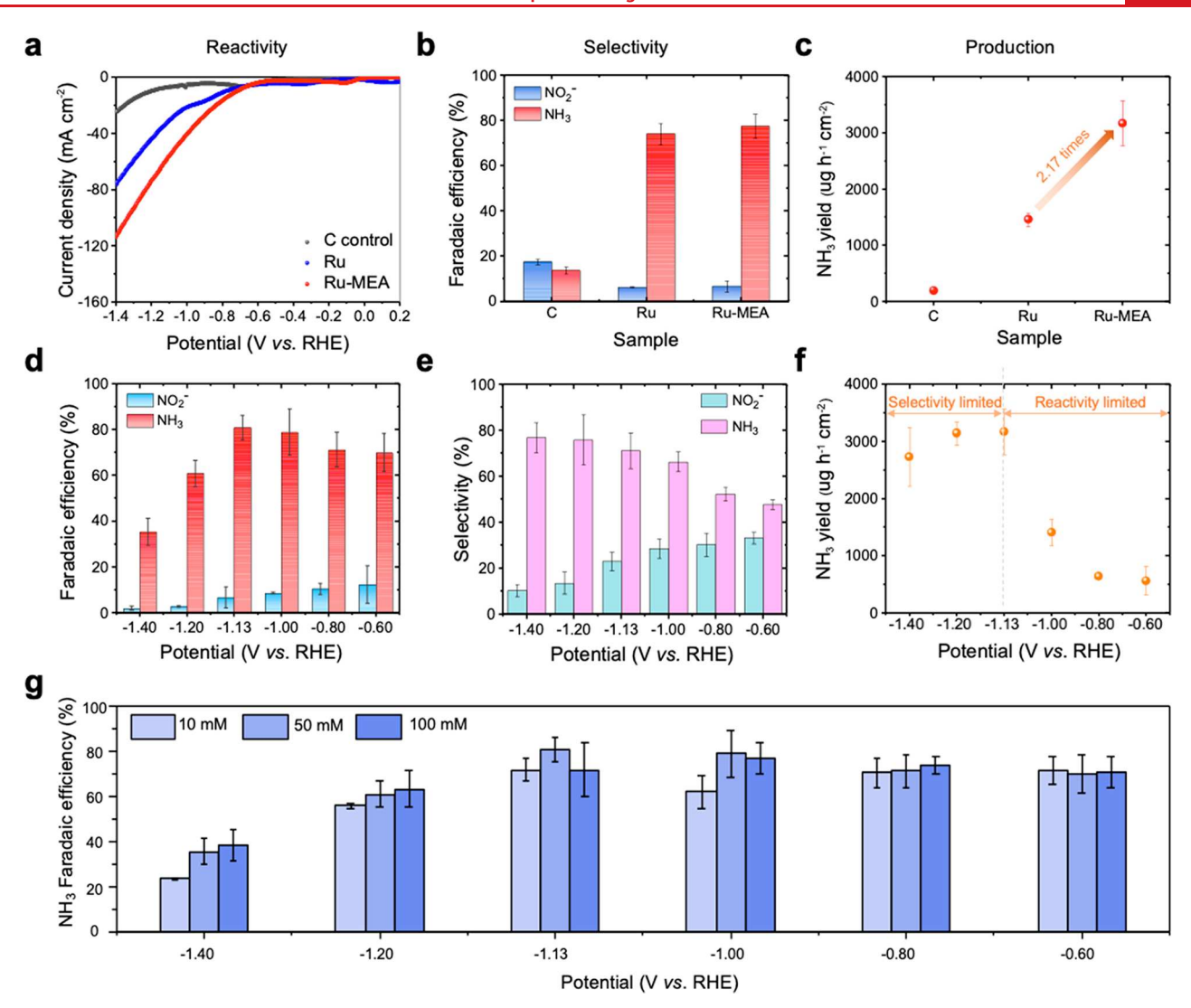


Figure 4. Key performance comparisons among different catalysts (C control, Ru, and Ru-MEA) in 0.5 M Na₂SO₄ containing 50 mM NO₃⁻, pH 2.5: (a) Linear sweep voltammetry (scan rate 5 mV s⁻¹). (b) FE_{NO2}^- and FE_{NH3} at -1.13 V vs RHE. (c) NH₃ yield (g h⁻¹ cm⁻²) at -1.13 V vs RHE. Electrocatalytic performance of Ru-MEA in 0.5 M Na₂SO₄ containing 50 mM NaNO₃, pH 2.5 at different applied potentials: (d) FE_{NH3} . (e) Selectivity toward NH₃ and NO₂⁻. (f) NH₃ yield (g h⁻¹ cm⁻²). Error bars indicate the standard deviation of the FE calculation from at least three independent samples. (g) FE_{NH3} of Ru-MEA catalyst with varying applied potentials and NO₃⁻ concentrations (10, 50, and 100 mM NO₃⁻) in moderate acidic media (pH 2.5).

coordination environment and electronic environments, allowing for the fine-tuning of adsorption energies suitable for various intermediate species in the ENR reaction.⁴⁹ Density functional theory (DFT) assisted by machine learning (ML) proved that the Ru site in the Ru-MEA benefited from a synergistic effect based on the free energy diagram, with the rate-limiting energy of 0.17 V vs -0.36 on Ru, resulting in enhanced ENR activity. By investigating the electrocatalytic behavior of Ru-MEA under different NO₃⁻ concentrations and applied potentials, the Ru-MEA NP catalyst exhibits a high NH₃ partial current density (i_{NH3}) of -50.8 mA cm⁻² (vs 26.8 mA cm⁻² by Ru) and a record-high NH₃ FE_{NH3} of 93.5% in an acidic condition relevant to industrial runoff in a flow cell reactor. In addition, under 3 h of continuous operation, the Ru-MEA showed only 19.0% decay in FE_{NH3}, much better than Ru (31.7% decay). This study paves the way toward developing next-generation electrocatalysts by combining novel synthesis and data-guided material designs for a range of applications.

The Ru-MEA NP catalyst was first synthesized on carbon paper substrates using a high-temperature thermal shock method (see Methods in the Supporting Information for details). The high-temperature shock (1200 K) leads to fast and complete decomposition of the precursor salts. Meanwhile, the short heating duration (~55 ms) along with the fast heating/cooling rates ensure the formation of a solid solution with a homogeneous elemental mixing state. Based on the composition screening calculations (Figures S1 and S2, Notes S1 and S2), the proposed Ru-MEA NPs should have a uniform dispersing of Ru with the Pt, Pd, and Cu metal elements, to form a cuboctahedralon particle. In addition to the Ru-MEA NPs, monometallic NPs (Ru, Cu, Pd, Pt) control samples were prepared using the same method (Figures S3–S5, Note S3).

A suite of characterizations was carried out to determine the structures of synthesized Ru-MEA NPs (see Methods for details). According to scanning transmission electron microscopy (STEM) energy-dispersive X-ray spectroscopy (EDX) (Figure 2a), no phase or elemental segregation was observed in

the Ru-MEA NPs. The four constituent elements were uniformly distributed. The high-angle annular dark-field (HAADF) image (Figure 2b) further revealed the formation of a face-centered-cubic (fcc) crystalline structure of the Ru-MEA NPs. The pristine carbon paper and synthesized Ru-MEA on carbon paper were compared using scanning electron microscope (SEM) (Figure S6). The mean radius of Ru-MEA NPs on carbon paper was identified as approximately 22.8 nm (Figure 2c) from a low magnification (10 000×) SEM (Figure S7). Moreover, the crystal structure identified from the powder X-ray diffraction (XRD) pattern (Figure 2d) confirmed the fcc structure, and small-angle X-ray scattering (SAXS) corresponded well with the XRD data. For Ru-MEA NPs synthesized with equally mixed precursor solutions, the bulk composition was determined using Inductively Coupled Plasma Mass Spectrometry (ICP-MS). The atomic ratio of Ru, Pt, Pd, and Cu was found to be 37%, 21%, 22%, and 20%, respectively. Additionally, the average atomic ratio at the surface or subsurface of Ru-MEA was characterized using X-ray photoelectron spectroscopy (XPS) and SEM-EDX based on three parallel samples (Table S1). This composition of MEA NPs is utilized for the following electrocatalytic tests. In addition, the valence states of the constituent elements were investigated by using XPS (Figure S8, Figures 2e-h). The three peaks of Pt $4f_{7/2}$ at about 71.35, 72.49, and 74.13 eV shown in Figure 2e show the oxidation of Pt. Figure 2f shows that Pd $3d_{5/2}$ was formed by Pd (0) $3d_{5/2}$, PdO $3d_{5/2}$, and PdO₂ 3d_{5/2} at 335.52, 337.32, and 338.88 eV, respectively. Figure 2g shows the Ru (0) 3d 5/2 peak centered at 279.94 eV. Cu 2p_{3/2} spectrum (Figure 2h) showed peaks at 933 and 934.52 eV, agreeing with the Cu (I) and Cu (0) oxidation states, along with a weak satellite peak at 945.94 eV, which indicates the valence state of +1. Note that the minor oxide components are likely due to surface oxidation of the NPs after synthesis.50 Details of the XPS peak fitting parameters are summarized in Table S2.

We performed first-principles DFT calculations to predict if the Ru-MEA could improve the activity for ENR compared to pure Ru. Due to its low energy (Note S4), we first investigated herein the ENR reaction activity on the RuPtPdCu (111) surface from Ru-MEA with an established atomistic structure shown in Figure S9. For ENR on Ru-MEA, we examined an eight-electron pathway as shown in Figure 3a, where NO₃⁻ will be first adsorbed on the metal surface, followed by reduction of the adsorbed NO₃⁻ to sequentially form NO₂, NO, and N.51-53 Finally, the formed N will be further protonated to form NH, NH₂, and the final product NH₃. Figure S10 shows the optimized adsorption configurations of all possible ENR intermediates on RuPtPdCu (111) surface, which agrees well with that on the unary hexagonal close packed (hcp) Ru (0001) (Figure S11) and fcc Cu (111) surface. 26 To efficiently analyze all the possible chemical species in Ru-MEA, we then applied a linear regression to correlate the DFT calculated adsorption energies for various chemical species involved in ENR on RuPtPdCu (111) with the chemical environments of the active sites (Figure 3b, Figure S12, and Note S5), with all fitting scores higher than 0.90. Table S3 shows that NO₃ reduction species are favorable to be adsorbed on the Ru atom of the RuPtPdCu (111) surface, as compared to the Cu, Pt, and Pd atoms, which proved our purpose of dispersing Ru in MEA components. This finding also reveals that the NO₃ reduction will predominantly occur on the site containing at least one Ru atom on the RuPtPdCu (111) surface.

Consequently, we believe that ENR will proceed on the Ru-MEA surface with the chemical environment having one Ru atom on the first neighboring site and random atom distribution on other neighboring sites, as shown in Figure S13. It is also inferred that the Ru-MEA catalyst should exhibit a similar ENR selectivity to metallic hcp Ru (0001), agreeing well with our observations (Figure 4) and previous reports.⁵⁴

To elaborate on the reaction mechanism and understand how synergistic function works on Ru-MEA NPs, we further applied DFT to calculate the free energy evolution for ENR to NO₂⁻, N₂, and NH₃ on both RuPtPdCu (111) and Ru (0001) surface using the computational hydrogen electrode method.⁵⁵ In Figure 3c, the desorption of *NO₂ requires a higher energy barrier than that of NO_2^- deoxidation, revealing that NO_2^- is a minor product of NO_3^- reduction on the RuPtPdCu (111) surface. Similarly, we predict that N is more energetically favorable to be protonated to form NH than dimerization of N to N₂. Therefore, the NH₃ product on Ru-MEA is predicted to be boosted via an eight-electron NO₃⁻ reduction reaction pathway. The limiting potential for ENR of Ru-MEA is predicted to be 0.17 V on the RuPtPdCu (111) surface with the corresponding rate-determining step being the protonation of N to form NH. The metallic hcp Ru (0001) surface shows a lower limiting potential of -0.36 eV to promote NO₃ reduction (Figure S14). This finding explains why Ru-MEA exhibits a higher ENR activity than the unary Ru catalyst. In addition, we examined the activity of competitive hydrogen evolution reaction (HER) to gauge ENR selectivity on Ru-MEA (Figure S15 and Note S6). By comparing the difference between the limiting potentials for ENR and HER (denoted as $U_L(ENR) - U_L(HER)$) on RuPtPdCu (111) (0.56 eV) and hcp Ru (0001) (0.07 eV), RuPtPdCu (111) is predicted to have a higher selectivity toward ENR. In conclusion, our DFT calculations predict enhanced selectivity of the Ru-MEA NPs catalyst for ENR.

The ENR activities of catalysts were investigated in a standard H-type cell with three electrodes (see Methods for details). An acidic electrolyte (pH 2.5) with 50 mM NO₃⁻ that mimics the industrial-level wastewater was selected for electrochemical measurements. The Ru-MEA catalyst showed a current density nearly 1.54 times higher than Ru (-63.7 mA cm^{-2} vs -41.4 mA cm^{-2}) at -1.13 V vs RHE (Figure 4a). Such an enhanced current density reflects higher ENR activity of Ru-MEA over Ru, consistent with DFT prediction. Ru-MEA increased the electrochemical surface areas (ECSA) than Ru (Figure S16 and Note S7), which has a positive effect on ENR activity. Notably, Ru-MEA features the highest activity among all catalyst compositions studied (Figure S17). In addition to the current density, the FE_{NH3} from monometallic catalysts (Cu, Pt, and Pd) was compared at a fixed potential (-1.13 V)vs RHE). As a result, Ru exhibited the highest NO₃ conversion rate and FE_{NH3}. It should be noted that even though the Cubased catalyst was reported to show high selectivity toward NH₃ in neutral medium,²¹ the unary Ru catalyst was measured to show higher NH3 selectivity than the unary Cu catalyst at an electrode potential of -1.13 V vs RHE in acid medium, agreeing well with our DFT prediction (Figure S19 and Note S8). In addition, Cu and Pd significantly contribute to enhancing the reaction activity, while the inclusion of Pt further improves the ENR activity of RuPdCu. Among all catalysts studied, the Ru-MEA catalyst showed the best FE_{NH3} of 79.8 \pm 5.8% (Figure 4b), which is also record-high among literature reports. Pure Ru also exhibited a comparable FE_{NH3}

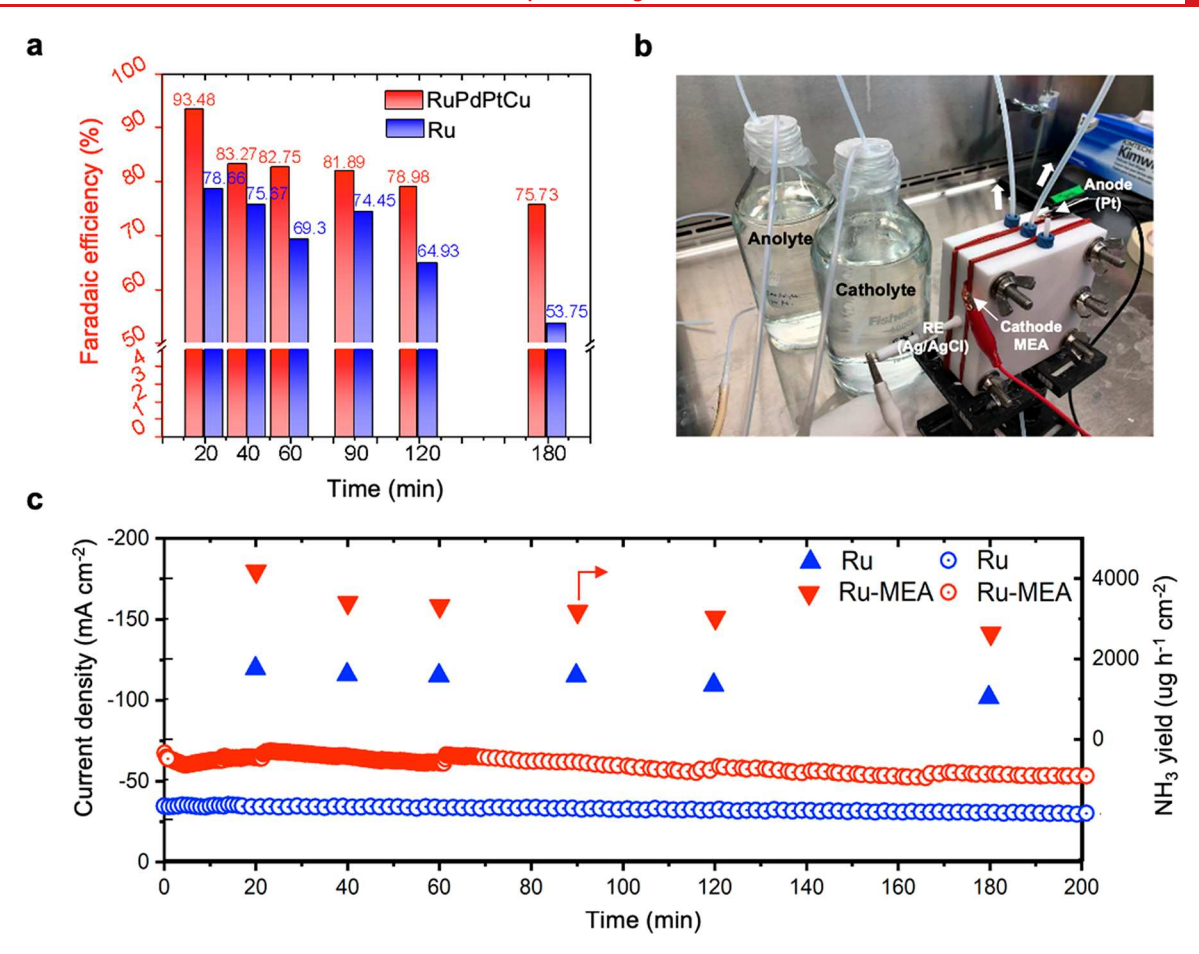


Figure 5. Stability test of Ru and Ru-MEA using a flow cell with fresh electrolyte (50 mM NO_3^- in 0.5 M Na_2SO_4 , pH 2.5), at -1.13 V vs. RHE, detailed design of the flow cell is in Figure S30: (a) FE_{NH3} of Ru and Ru-MEA. The FE_{NH3} of Ru-MEA remains above 75% for the 200 min test, whereas the FE_{NH3} at 20 min is 93.5%. (b) Photo of the electrocatalytic flow cell. (c) Current density (mA cm⁻²) and NH_3 yield (ug h⁻¹ cm⁻²) of Ru and Ru-MEA.

of 71.9 \pm 2.6%, representing its intrinsic good NH₃ selectivity. As a result of enhanced current density and FE_{NH3}, the Ru-MEA catalyst doubled the NH₃ yield (3171.0 μ g h $^{-1}$ cm $^{-2}$) compared to pure Ru (1461.2 μ g h $^{-1}$ cm $^{-2}$) (Figure 4c), which proved the DFT calculation that ENR is promoted on Ru-MEA surface with the chemical environment having one Ru atom on the first neighboring site and random atom distribution on other neighboring sites.

We then investigated the FE_{NH3} of Ru-MEA with varying applied potentials. For ENR in 50 mM NO₃⁻ (Figure 4d), with decreasing applied potentials, the FE_{NH3} first increased and then gradually decreased. For applied potential between -0.60V and -1.13 V vs RHE, the FE_{NH3} increased as the reduction was promoted, while NO2- and other intermediate species were reduced into NH₃. The measured optimized potential was at -1.13 V vs RHE, exhibiting a FE_{NH3} of 79.8% \pm 5.8%. When the applied potential was further reduced, the effect of competing hydrogen evolution reaction (HER) became more significant, thus reducing FE_{NH3}. 56 As the potential decreased, the selectivity of NH3 increased and the selectivity of the toxic byproduct NO₂⁻ decreased accordingly (Figure 4e). At the optimum condition (-1.13 V vs RHE), the NH₃ selectivity was 71.15%, and selectivity toward NO2 was approximately 23.07%, the reaction consistent with first-order kinetics (Figure S20 and Note S9).

ENR performance on Ru-MEA was also investigated with different NO₃⁻ concentrations. In addition to 50 mM NO₃⁻,

10 mM and 100 mM NO₃⁻ were considered to cover the range of other types of NO₃⁻-containing wastewater at the source of generation, such as textile wastewater and nuclear industry. 17,57-59 NO₃ reduction was hindered by competition reaction, mainly HER, especially for low NO₃⁻ concentration; however, a proton is necessary for the NO₃⁻ reduction. At 10 mM NO₃⁻, the FE_{NH3} went through a peak with applied potential since mass transport of NO₃⁻ becomes the limiting factor, even for more negative potentials (Figure S21). This trend can be further proved with higher NO₃⁻ concentration (Figures S22–23), and when there is more NO_3^- available in the electrolyte, mass transport becomes less limiting for the $\mathrm{NO_3}^-$ reduction reaction. However, the higher $\mathrm{FE}_{\mathrm{NH3}}$ at high NO₃⁻ concentrations (100 mM NO₃⁻) compared to 50 mM NO₃⁻ under more negative potential is most likely due to the competitive adsorption of protons with the NO₃⁻ ion (Figure 4g) considering the Ru site is preferred for both NO₃⁻ and *H species (Table S3). In addition, overall FE_{NO2}- increased with a higher initial NO₃⁻ concentration, contributing to further NO₂⁻ degradation. Since the availability of active sites mainly limits reaction kinetics, NO₂⁻ reduction is understandably less efficient than NO3- reduction due to the lack of active adsorption sites for NO2- and available *H on adjacent sites, leading to NO2- desorption and accumulation in the electrolyte. Lastly, when considering the ENR performance at a specific NO₃⁻ concentration, the FE_{NH3} was found to increase with more negative applied potential due to the

enhanced reducing power, which has a higher impact on ENR compared to that on HER. When applied potential became more negative, the HER became dominant, which was observed by the increasing $FE_{\rm H2}$ in Figures S21–23.

We compared the electrochemical stability of Ru and Ru-MEA catalysts using chronoamperometry (CA) at -1.13 V vs RHE with 50 mM NO₃⁻ in a flow cell (Methods, Figure 5b, Figure S30). For Ru, the initial FE_{NH3} was at an average of 74.5% for the first hour with an NH3 partial current density (i_{NH3}) of 24.2 mA cm⁻². However, the performance decayed over time and dropped to 53.8% at around 180 min, followed by a further decline in the following hours (Figure 5a). In contrast, the Ru-MEA catalyst demonstrated a much higher FE_{NH3} at 93.5% in the first 20 min. Though the FE_{NH3} also slightly decreased in the following hours, the value remained high and relatively stable (75.7%) until 180 min (Figure 5a), along with a high i_{NH3} of 42.8 mA cm⁻² (Figure 5c). Tables S4 and S5 summarize the up-to-date reported highest FE_{NH3} under the different conditions, where our Ru-MEA catalyst stands out. The decline in FE_{NH3} may be caused by several factors. For example, metal corrosion and leaching may cause catalyst composition change and affect sample performance, which has been reported and is hard to avoid. 60-62 Material poisoning caused by strong adsorption energy between active sites and intermediates may cause temporary or permanent loss of reaction sites for ENR. Particle aggregation and nanostructure change will also cause an irreversible change of catalysts' morphology. To understand these effects, we characterized the surface elemental composition (Figures S24-25), catalyst morphology (Figures S26-27), and crystal structure (Figure S28) of Ru-MEA after a 4 h stability test. While the crystal structure and the composition remained relatively stable, we observed a notable decrease in the number of NPs on the carbon paper surface (e.g., 169 to 107, Figure S27), suggesting detachment issues. We further utilized ICP-MS to analyze the electrolyte after the test (details in the Supporting Information), and the results revealed a loss of 12.8 wt % of Cu and 6.8 wt % of Ru in the initial catalyst during the ENR process. The losses of Cu and Ru were also shown by the SEM-EDX analysis of the catalysts after the stability test (Table S6). Direct NO₃⁻ reduction in an acidic environment has historically been a challenging process due to catalyst leaching issues. Therefore, to enhance the stability of catalysts, we incorporated a binder of 20 wt.% Nafion. With the binder, we observed that the current density changed by less than 8% within 3 h, vs 16.8% without the binder (Figure S29). Nevertheless, this Ru-MEA catalyst design for the first time enables highly selective ENR to NH₃ in acidic solutions with record-high FE_{NH3} and better stability compared to benchmark Ru catalysts.

This study for the first time reported a MEA NP catalyst designed for efficient ENR toward NH₃ with dispersed Ru sites and synergy between Ru and Pd, Pt, and Cu. A simple thermal shock method achieved solid-solution-level mixing of Ru in the MEA NPs. DFT assisted by ML predicted the enhanced ENR activity and NH₃ selectivity on Ru-MEA NPs compared to the benchmark Ru catalyst, exploiting the synergistic effect of the components to provide optimized multistep NO₃⁻ reduction energy. The resulting Ru-MEA NP catalyst exhibits record high FE_{NH3} in acidic conditions among existing catalysts and superior stability compared with the Ru. This work demonstrated a rational catalyst discovery pathway by integrating novel synthesis and DFT-guided design toward a

range of applications related to sustainability. In future studies, the critical masses of Pt and Pd need to be optimized and the composition of the designed MEA could be extended to economically more viable components (e.g., non-noble metals). In addition, considering the cost of catalysts and pretreatment of acidic wastewater, a thorough technoeconomic analysis would be necessary to ensure a practical and economically viable solution for treating acidic wastewater. It needs to be acknowledged that the catalyst loading for this study is relatively lower (2 wt %) than existing studies; with a potential improvement of the catalyst loading, the NH₃ yield has the potential for a significant increment to satisfy the practical requirements. In addition, Ru-MEA must be tested in real NO₃⁻-containing wastewater with various coexisting components.

ASSOCIATED CONTENT

Supporting Information

The Supporting Information is available free of charge at https://pubs.acs.org/doi/10.1021/acs.nanolett.3c01978.

Experimental details and supporting figures and tables; information on the materials synthesis; DFT calculation; sample characterizations; ECSA measurement of Ru-MEA and Ru; ENR performance of Ru-MEA and single-component and ternary-component nanoparticles; SEM, elemental mapping, TEM, and XPS characterizations of Ru-MEA and single-component nanoparticles (PDF)

AUTHOR INFORMATION

Corresponding Authors

Zhiyong Jason Ren — Department of Civil and Environmental Engineering and Andlinger Center for Energy and the Environment, Princeton University, Princeton, New Jersey 08544, United States; orcid.org/0000-0001-7606-0331; Email: zjren@princeton.edu

Guofeng Wang — Department of Mechanical Engineering and Materials Science, University of Pittsburgh, Pittsburgh, Pennsylvania 15260, United States; oorcid.org/0000-0001-8249-4101; Email: guw8@pitt.edu

Liangbing Hu − Department of Materials Science and Engineering, University of Maryland, College Park, Maryland 20742, United States; orcid.org/0000-0002-9456-9315; Email: binghu@umd.edu

Authors

Meiqi Yang — Department of Civil and Environmental Engineering and Andlinger Center for Energy and the Environment, Princeton University, Princeton, New Jersey 08544, United States; orcid.org/0000-0003-0913-6804

Boyang Li – Department of Mechanical Engineering and Materials Science, University of Pittsburgh, Pittsburgh, Pennsylvania 15260, United States

Shuke Li — Department of Materials Science and Engineering, University of Maryland, College Park, Maryland 20742, United States

Qi Dong – Department of Materials Science and Engineering, University of Maryland, College Park, Maryland 20742, United States

Zhennan Huang — Department of Materials Science and Engineering, University of Maryland, College Park, Maryland 20742, United States

- Sunxiang Zheng Department of Civil and Environmental Engineering and Andlinger Center for Energy and the Environment, Princeton University, Princeton, New Jersey 08544, United States
- Ying Fang Department of Mechanical Engineering and Materials Science, University of Pittsburgh, Pittsburgh, Pennsylvania 15260, United States
- Guangye Zhou Department of Civil and Environmental Engineering and Andlinger Center for Energy and the Environment, Princeton University, Princeton, New Jersey 08544, United States
- Xi Chen Department of Civil and Environmental
 Engineering and Andlinger Center for Energy and the
 Environment, Princeton University, Princeton, New Jersey
 08544, United States; orcid.org/0000-0003-2360-2672
- Xiaobo Zhu Department of Civil and Environmental Engineering and Andlinger Center for Energy and the Environment, Princeton University, Princeton, New Jersey 08544, United States
- Tangyuan Li Department of Materials Science and Engineering, University of Maryland, College Park, Maryland 20742, United States
- Miaofang Chi Center for Nanophase Materials Sciences, Oak Ridge National Laboratory, Oak Ridge, Tennessee 37932, United States; oorcid.org/0000-0003-0764-1567

Complete contact information is available at: https://pubs.acs.org/10.1021/acs.nanolett.3c01978

Author Contributions

[†]M.Y., B.L., and S.L. contributed equally to this work. M.Y., L.H., G.W., and Z.J.R conceived the design of the project and initiated the project. S.L. and T.L. were in charge of catalyst synthesis. M.Y. performed most of the material characterization and electrochemical measurements. M.Y. performed SEM and XPS measurements and data analysis. Z.H. performed TEM measurements and data analysis. S.Z. performed XRD measurements and data analysis. All electrochemical data were collected, analyzed, and interpreted by M.Y. and Q.D. G.Z. performed the stability test. B.L. performed the DFT calculations. Y.F. performed the machine learning model predictions. All authors contributed to discussions. M.Y. wrote the paper with inputs from the other authors, and D.Q., X.Z., and X.C. revised the manuscript. All authors reviewed the paper. L.H., G.W., and Z.J.R. supervised the research.

Notes

The authors declare no competing financial interest.

ACKNOWLEDGMENTS

This work was supported by Princeton Catalysis Initiative (PCI). We acknowledge the use of the PRISM Image and Analysis Center (IAC) at Princeton University. B.L. and G.W. acknowledge the support from U.S. National Science Foundation (NSF DMR #1905572). Z.H. and M.C. were supported by the U.S. DOE, Office of BES, Chemical Sciences, Geosciences, and Biosciences Division, Catalysis Science program. Microscopy work was performed at the Center for Nanophase Materials Sciences, which is a U.S. DOE Office of Science User Facility at Oak Ridge National Laboratory.

REFERENCES

- (1) Galloway, J. N.; Townsend, A. R.; Erisman, J. W.; Bekunda, M.; Cai, Z.; Freney, J. R.; Martinelli, L. A.; Seitzinger, S. P.; Sutton, M. A. Transformation of the Nitrogen Cycle. *Science* (80-.) **2008**, 320 (May), 889–892.
- (2) Stevens, C. J. Nitrogen in the Environment. *Science* (80-.) **2019**, 363 (6427), 578–580.
- (3) Padilla, F. M.; Gallardo, M.; Manzano-Agugliaro, F. Global Trends in Nitrate Leaching Research in the 1960–2017 Period. *Sci. Total Environ.* **2018**, *643* (2), 400–413.
- (4) Lundberg, J. O.; Weitzberg, E.; Cole, J. A.; Benjamin, N. Nitrate, Bacteria and Human Health. *Nat. Rev. Microbiol.* **2004**, 2 (7), 593–602
- (5) Archna; Sharma, S. K.; Sobti, R. C. Nitrate Removal from Ground Water: A Review. *E-Journal Chem.* **2012**, 9 (4), 1667–1675.
- (6) Sperl, G. T.; Hoare, D. S. Denitrification with Methanol: A Selective Enrichment for Hyphomicrobium Species. *J. Bacteriol.* **1971**, 108 (2), 733–736.
- (7) Timmermans, P.; Van Haute, A. Denitrification with Methanol. Fundamental Study of the Growth and Denitrification Capacity of Hyphomicrobium Sp. *Water Res.* 1983, *17* (10), 1249–1255.
- (8) Beaulieu, J. J.; Tank, J. L.; Hamilton, S. K.; Wollheim, W. M.; Hall, R. O.; Mulholland, P. J.; Peterson, B. J.; Ashkenas, L. R.; Cooper, L. W.; Dahm, C. N.; et al. Nitrous Oxide Emission from Denitrification in Stream and River Networks. *Proc. Natl. Acad. Sci. U. S. A.* 2011, 108 (1), 214–219.
- (9) Glass, C.; Silverstein, J. Denitrification of High-Nitrate, High-Salinity Wastewater. *Water Res.* **1999**, 33 (1), 223–229.
- (10) Goyal, A.; Srivastava, V. C. Treatment of Highly Acidic Wastewater Containing High Energetic Compounds Using Dimensionally Stable Anode. *Chem. Eng. J.* **2017**, 325, 289–299.
- (11) Nancharaiah, Y. V.; Krishna Mohan, T. V.; Satya Sai, P. M.; Venugopalan, V. P. Denitrification of High Strength Nitrate Bearing Acidic Waters in Granular Sludge Sequencing Batch Reactors. *Int. Biodeterior. Biodegrad.* **2017**, *119*, 28–36.
- (12) Ma, H.; Shen, M.; Tong, Y.; Wang, X. Radioactive Wastewater Treatment Technologies: A Review. *Molecules* **2023**, 28 (4), 1935.
- (13) Bird, F.; Clarke, A.; Davies, P.; Surkovic, E. Ammonia: Zero-Carbon Fertiliser, Fuel and Energy Store: The Royal Society; 2020.
- (14) MacFarlane, D. R.; Cherepanov, P. V.; Choi, J.; Suryanto, B. H. R.; Hodgetts, R. Y.; Bakker, J. M.; Ferrero Vallana, F. M.; Simonov, A. N. A Roadmap to the Ammonia Economy. *Joule* **2020**, *4* (6), 1186–1205.
- (15) Van Damme, M.; Clarisse, L.; Whitburn, S.; Hadji-Lazaro, J.; Hurtmans, D.; Clerbaux, C.; Coheur, P. F. Industrial and Agricultural Ammonia Point Sources Exposed. *Nature* **2018**, *564* (7734), 99–103.
- (16) Zeng, Y.; Priest, C.; Wang, G.; Wu, G. Restoring the Nitrogen Cycle by Electrochemical Reduction of Nitrate: Progress and Prospects. *Small Methods* **2020**, *4*, 2000672.
- (17) Van Langevelde, P. H.; Katsounaros, I.; Koper, M. T. M. Ll Electrocatalytic Nitrate Reduction for Sustainable Ammonia Production. *Joule* **2021**, *5*, 290–294.
- (18) Zhu, J. J.; Dressel, W.; Pacion, K.; Ren, Z. J. ES&T in the 21st Century: A Data-Driven Analysis of Research Topics, Interconnections, and Trends in the Past 20 Years. *Environ. Sci. Technol.* **2021**, 55 (6), 3453–3464.
- (19) Liu, J. X.; Richards, D.; Singh, N.; Goldsmith, B. R. Activity and Selectivity Trends in Electrocatalytic Nitrate Reduction on Transition Metals. *ACS Catal* **2019**, *9* (8), 7052–7064.
- (20) Wang, Z.; Richards, D.; Singh, N. Recent Discoveries in the Reaction Mechanism of Heterogeneous Electrocatalytic Nitrate Reduction. *Catal. Sci. Technol.* **2021**, *11* (3), 705–725.
- (21) Zhao, Y.; Liu, Y.; Zhang, Z.; Mo, Z.; Wang, C.; Gao, S. Flower-like Open-Structured Polycrystalline Copper with Synergistic Multi-Crystal Plane for Efficient Electrocatalytic Reduction of Nitrate to Ammonia. *Nano Energy* **2022**, *97*, 107124.
- (22) Chen, C.; Li, K.; Li, C.; Sun, T.; Jia, J. Combination of Pd-Cu Catalysis and Electrolytic H2 Evolution for Selective Nitrate

- Reduction Using Protonated Polypyrrole as a Cathode. *Environ. Sci. Technol.* **2019**, 53 (23), 13868–13877.
- (23) Duca, M.; Sacré, N.; Wang, A.; Garbarino, S.; Guay, D. Enhanced Electrocatalytic Nitrate Reduction by Preferentially-Oriented (100) PtRh and PtIr Alloys: The Hidden Treasures of the Miscibility Gap. Appl. Catal. B Environ. 2018, 221 (100), 86–96.
- (24) Kato, M.; Okui, M.; Taguchi, S.; Yagi, I. Electrocatalytic Nitrate Reduction on Well-Defined Surfaces of Tin-Modified Platinum, Palladium and Platinum-Palladium Single Crystalline Electrodes in Acidic and Neutral Media. *J. Electroanal. Chem.* **2017**, 800 (2), 46–53.
- (25) Wang, Z.; Young, S. D.; Goldsmith, B. R.; Singh, N. Increasing Electrocatalytic Nitrate Reduction Activity by Controlling Adsorption through PtRu Alloying. *J. Catal.* **2021**, 395 (3), 143–154.
- (26) Wang, Y.; Xu, A.; Wang, Z.; Huang, L.; Li, J.; Li, F.; Wicks, J.; Luo, M.; Nam, D. H.; Tan, C. S.; Ding, Y.; Wu, J.; Lum, Y.; Dinh, C. T.; Sinton, D.; Zheng, G.; Sargent, E. H. Enhanced Nitrate-to-Ammonia Activity on Copper-Nickel Alloys via Tuning of Intermediate Adsorption. *J. Am. Chem. Soc.* 2020, 142 (12), 5702–5708.
- (27) Santos, A. S. G. G.; Restivo, J.; Orge, C. A.; Pereira, M. F. R.; Soares, O. S. G. P. Nitrate Catalytic Reduction over Bimetallic Catalysts: Catalyst Optimization. *C* **2020**, *6* (4), 78.
- (28) She, Z. W.; Kibsgaard, J.; Dickens, C. F.; Chorkendorff, I.; Nørskov, J. K.; Jaramillo, T. F. Combining Theory and Experiment in Electrocatalysis: Insights into Materials Design. *Science* (80-.) **2017**, No. 6321, 355.
- (29) Ding, J.; Li, W.; Zhao, Q. L.; Wang, K.; Zheng, Z.; Gao, Y. Z. Electroreduction of Nitrate in Water: Role of Cathode and Cell Configuration. *Chem. Eng. J.* **2015**, *271*, 252–259.
- (30) Huang, L.; Cheng, L.; Ma, T.; Zhang, J.; Wu, H.; Su, J.; Song, Y.; Zhu, H.; Liu, Q.; Zhu, M.; et al. Direct Synthessis of Ammonia From Nitrate On Amorphous Graphene With Near 100% Efficiency. *Adv. Mater.* 2023, 2211856, 2211856.
- (31) Zhu, W.; Zhang, X.; Yin, Y.; Qin, Y.; Zhang, J.; Wang, Q. In-Situ Electrochemical Activation of Carbon Fiber Paper for the Highly Efficient Electroreduction of Concentrated Nitric Acid. *Electrochim. Acta* 2018, 291, 328–334.
- (32) Li, P.; Jin, Z.; Fang, Z.; Yu, G. A Single-Site Iron Catalyst with Preoccupied Active Centers That Achieves Selective Ammonia Electrosynthesis from Nitrate. *Energy Environ. Sci.* **2021**, *14*, 3522.
- (33) Yang, B.; Ding, W.; Zhang, H.; Zhang, S. Recent Progress in Electrochemical Synthesis of Ammonia from Nitrogen: Strategies to Improve the Catalytic Activity and Selectivity. *Energy Environ. Sci.* **2021**, *14* (2), 672–687.
- (34) Xi, J.; Jung, H. S.; Xu, Y.; Xiao, F.; Bae, J. W.; Wang, S. Single-Atom Catalysts: Synthesis Strategies, Catalytic Applications, and Performance Regulation of Single-Atom Catalysts (Adv. Funct. Mater. 12/2021). *Adv. Funct. Mater.* 2021, 31 (12), 2170081.
- (35) McEnaney, J. M.; Blair, S. J.; Nielander, A. C.; Schwalbe, J. A.; Koshy, D. M.; Cargnello, M.; Jaramillo, T. F. Electrolyte Engineering for Efficient Electrochemical Nitrate Reduction to Ammonia on a Titanium Electrode. ACS Sustain. Chem. Eng. 2020, 8 (7), 2672–2681.
- (36) Watanabe, T.; Jin, H. W.; Cho, K. J.; Kuroda, M. Application of a Bio-Electrochemical Reactor Process to Direct Treatment of Metal Pickling Wastewater Containing Heavy Metals and High Strength Nitrate. *Water Sci. Technol.* **2004**, *50* (8), 111–118.
- (37) Regel-Rosocka, M. A Review on Methods of Regeneration of Spent Pickling Solutions from Steel Processing. *J. Hazard. Mater.* **2010**, *177* (1–3), 57–69.
- (38) Huo, X.; Van Hoomissen, D. J.; Liu, J.; Vyas, S.; Strathmann, T. J. Hydrogenation of Aqueous Nitrate and Nitrite with Ruthenium Catalysts. *Appl. Catal. B Environ.* **2017**, *211*, 188–198.
- (39) Li, J.; Zhan, G.; Yang, J.; Quan, F.; Mao, C.; Liu, Y.; Wang, B.; Lei, F.; Li, L.; Chan, A. W. M.; Xu, L.; Shi, Y.; Du, Y.; Hao, W.; Wong, P. K.; Wang, J.; Dou, S. X.; Zhang, L.; Yu, J. C. Efficient Ammonia Electrosynthesis from Nitrate on Strained Ruthenium Nanoclusters. J. Am. Chem. Soc. 2020, 142 (15), 7036–7046.

- (40) Chen, G. F.; Yuan, Y.; Jiang, H.; Ren, S. Y.; Ding, L. X.; Ma, L.; Wu, T.; Lu, J.; Wang, H. Electrochemical Reduction of Nitrate to Ammonia via Direct Eight-Electron Transfer Using a Copper–Molecular Solid Catalyst. *Nat. Energy* **2020**, *5*, 605.
- (41) Chen, F. Y.; Wu, Z. Y.; Gupta, S.; Rivera, D. J.; Lambeets, S. V.; Pecaut, S.; Kim, J. Y. T.; Zhu, P.; Finfrock, Y. Z.; Meira, D. M.; King, G.; Gao, G.; Xu, W.; Cullen, D. A.; Zhou, H.; Han, Y.; Perea, D. E.; Muhich, C. L.; Wang, H. Efficient Conversion of Low-Concentration Nitrate Sources into Ammonia on a Ru-Dispersed Cu Nanowire Electrocatalyst. *Nat. Nanotechnol.* **2022**, *17* (7), 759–767.
- (42) Huang, B.; Kobayashi, H.; Yamamoto, T.; Matsumura, S.; Nishida, Y.; Sato, K.; Nagaoka, K.; Kawaguchi, S.; Kubota, Y.; Kitagawa, H. Solid-Solution Alloying of Immiscible Ru and Cu with Enhanced CO Oxidation Activity. *J. Am. Chem. Soc.* **2017**, *139* (13), 4643–4646.
- (43) Yang, C.; Ko, B. H.; Hwang, S.; Liu, Z.; Yao, Y.; Luc, W.; Cui, M.; Malkani, A. S.; Li, T.; Wang, X.; Dai, J.; Xu, B.; Wang, G.; Su, D.; Jiao, F.; Hu, L. Overcoming Immiscibility toward Bimetallic Catalyst Library. *Sci. Adv.* **2020**, *6* (17), 1–10.
- (44) Barrabés, N.; Just, J.; Dafinov, A.; Medina, F.; Fierro, J. L. G.; Sueiras, J. E.; Salagre, P.; Cesteros, Y. Catalytic Reduction of Nitrate on Pt-Cu and Pd-Cu on Active Carbon Using Continuous Reactor: The Effect of Copper Nanoparticles. *Appl. Catal. B Environ.* **2006**, *62* (1–2), 77–85.
- (45) Sarker, A. C.; Kato, M.; Yagi, I. Electrocatalytic Nitrate and Nitrous Oxide Reduction at Interfaces between Pt-Pd Nanoparticles and Fluorine-Doped Tin Oxide. *Electrochim. Acta* **2022**, *425* (3), 140628
- (46) Gao, Q.; Pillai, H. S.; Huang, Y.; Liu, S.; Mu, Q.; Han, X.; Yan, Z.; Zhou, H.; He, Q.; Xin, H.; Zhu, H. Breaking Adsorption-Energy Scaling Limitations of Electrocatalytic Nitrate Reduction on Intermetallic CuPd Nanocubes by Machine-Learned Insights. *Nat. Commun.* 2022, 13 (1), 1–12.
- (47) Lim, J.; Chen, Y.; Cullen, D. A.; Lee, S. W.; Senftle, T. P.; Hatzell, M. C. PdCu Electrocatalysts for Selective Nitrate and Nitrite Reduction to Nitrogen. *ACS Catal* **2023**, *13* (1), 87–98.
- (48) Yao, Y.; Huang, Z.; Xie, P.; Lacey, S. D.; Jacob, R. J.; Xie, H.; Chen, F.; Nie, A.; Pu, T.; Rehwoldt, M.; Yu, D.; Zachariah, M. R.; Wang, C.; Shahbazian-Yassar, R.; Li, J.; Hu, L. Carbothermal Shock Synthesis of High-Entropy-Alloy Nanoparticles. *Science* (80-.) 2018, 359 (6383), 1489–1494.
- (49) Li, H.; Lai, J.; Li, Z.; Wang, L. Multi-Sites Electrocatalysis in High-Entropy Alloys. *Adv. Funct. Mater.* **2021**, *31* (47), 2106715.
- (50) Miyashita, S.; Wakisaka, M.; Iiyama, A.; Uchida, H. Analysis of the Surface Oxidation Process on Pt Nanoparticles on a Glassy Carbon Electrode by Angle-Resolved, Grazing-Incidence X-Ray Photoelectron Spectroscopy. *Langmuir* **2017**, *33* (36), 8877–8882.
- (51) Pérez-Gallent, E.; Figueiredo, M. C.; Katsounaros, I.; Koper, M. T. M. Electrocatalytic Reduction of Nitrate on Copper Single Crystals in Acidic and Alkaline Solutions. *Electrochim. Acta* **2017**, 227, 77–84.
- (52) Katsounaros, I.; Figueiredo, M. C.; Chen, X.; Calle-Vallejo, F.; Koper, M. T. M. Interconversions of Nitrogen-Containing Species on Pt(100) and Pt(111) Electrodes in Acidic Solutions Containing Nitrate. *Electrochim. Acta* **2018**, 271, 77–83.
- (53) Katsounaros, I.; Figueiredo, M. C.; Chen, X.; Calle-Vallejo, F.; Koper, M. T. M. Structure- and Coverage-Sensitive Mechanism of NO Reduction on Platinum Electrodes. *ACS Catal* **2017**, *7* (7), 4660–4667.
- (54) Zeng, Y.; Priest, C.; Wang, G.; Wu, G. Restoring the Nitrogen Cycle by Electrochemical Reduction of Nitrate: Progress and Prospects. *Small Methods* **2020**, *4* (12), 2000672.
- (55) Nørskov, J. K.; Rossmeisl, J.; Logadottir, A.; Lindqvist, L.; Kitchin, J. R.; Bligaard, T.; Jónsson, H. Origin of the Overpotential for Oxygen Reduction at a Fuel-Cell Cathode. *J. Phys. Chem. B* **2004**, *108* (46), 17886–17892.
- (56) Wang, Y.; Zhou, W.; Jia, R.; Yu, Y.; Zhang, B. Unveiling the Activity Origin of a Copper-Based Electrocatalyst for Selective Nitrate Reduction to Ammonia. *Angew. Chemie Int. Ed.* **2020**, *59* (13), 5350–5354.

- (57) Chauhan, R.; Srivastava, V. C. Electrochemical Denitrification of Highly Contaminated Actual Nitrate Wastewater by Ti/RuO2 Anode and Iron Cathode. Chem. Eng. J. 2020, 386 (3), 122065.
- (58) Clifford, D.; Liu, X. Biological Denitrification of Spent Regenerant Brine Using a Sequencing Batch Reactor. Water Res. **1993**, 27 (9), 1477–1484.
- (59) Hou, D.; Iddya, A.; Chen, X.; Wang, M.; Zhang, W.; Ding, Y.; Jassby, D.; Ren, Z. J. Nickel-Based Membrane Electrodes Enable High-Rate Electrochemical Ammonia Recovery. Environ. Sci. Technol. **2018**, 52 (15), 8930–8938.
- (60) Zhang, J.; Quast, T.; He, W.; Dieckhöfer, S.; Junqueira, J. R. C.; Öhl, D.; Wilde, P.; Jambrec, D.; Chen, Y. T.; Schuhmann, W. In Situ Carbon Corrosion and Cu Leaching as a Strategy for Boosting Oxygen Evolution Reaction in Multimetal Electrocatalysts. Adv. Mater. 2022, 34 (13), 2109108.
- (61) Strasser, P.; Kühl, S. Dealloyed Pt-Based Core-Shell Oxygen Reduction Electrocatalysts. Nano Energy 2016, 29, 166-177.
- (62) Chen, S.; Niu, Z.; Xie, C.; Gao, M.; Lai, M.; Li, M.; Yang, P. Effects of Catalyst Processing on the Activity and Stability of Pt-Ni Nanoframe Electrocatalysts. ACS Nano 2018, 12 (8), 8697-8705.

□ Recommended by ACS

Pulsed Nitrate-to-Ammonia Electroreduction Facilitated by **Tandem Catalysis of Nitrite Intermediates**

Panpan Li, Guihua Yu, et al.

MARCH 10, 2023

JOURNAL OF THE AMERICAN CHEMICAL SOCIETY

READ **C**

Efficient Electrocatalytic Nitrate Reduction to Ammonia Based on DNA-Templated Copper Nanoclusters

Wenjie Luo, Zhi Yang, et al.

APRIL 04, 2023

ACS APPLIED MATERIALS & INTERFACES

READ **C**

Ambient Ammonia Synthesis via Nitrate Electroreduction in Neutral Media on Fe₃O₄ Nanoparticles-decorated TiO₅ **Nanoribbon Array**

Xun He, Xuping Sun, et al.

DECEMBER 20, 2022

INORGANIC CHEMISTRY

READ **C**

Potential Dependence of Ammonia Selectivity of **Electrochemical Nitrate Reduction on Copper Oxide**

Rong Yang, Jianping Xiao, et al.

OCTOBER 19, 2022

ACS SUSTAINABLE CHEMISTRY & ENGINEERING

READ **C**

Get More Suggestions >